Synthesis and Biological Activity of Ni(II), La(III), and Ce(IV) Complexes with 8-Hydroxy-7-iodo-6-((4-sulfophenyl)diazinyl)quinoline-5-sulfonic Acid Ligand

Noora Qasem Muhi* **and Alyaa Khider Abbas**

Department of Chemistry, College of Science, University of Baghdad, Al Jadriya Street, Baghdad 10071, Iraq

** **Corresponding author:***

email:
nora.qasem1605a@sc.uobaghdad.edu.iq

Received: August 21, 2025
Accepted: October 13, 2025

DOI: 10.22146/ijc.110573

Abstract: *In this study, a new azo ligand, 8-hydroxy-7-iodo-6-((4-sulfophenyl)diazinyl)quinoline-5-sulfonic acid (HAQ), was synthesized from 8-hydroxy-7-iodo-quinoline-5-sulfonic acid using a diazotization-coupling procedure and then complexed with La(III), Ni(II), and Ce(IV) ions. The ligand and its metal complexes were analyzed using elemental analysis, FTIR, UV-vis, ^{1}H-NMR, TGA, SEM, ICP, and XRD techniques. Spectral and analytical results indicated the effective coordination of oxygen and nitrogen donor atoms, resulting in stable 1:1 (metal:ligand) of $[La(HAQ)Cl_2(H_2O)_2]\cdot 5H_2O$, and (1:2) of $[Ce(HAQ)_2(SO_4)]\cdot H_2O$ and $[Ni(HAQ)_2(H_2O)_2]\cdot 4H_2O$ complexes. Thermal analysis has revealed that metal complexes are more thermally stable than their corresponding free ligands. SEM showed significant morphological modifications during complexation, whereas XRD patterns revealed an increase in crystallinity in the metal complexes. The antioxidant characteristics of the synthesized compounds were evaluated using the phosphomolybdate technique, with the Ce(IV) complex displaying the highest activity, most likely due to its redox capacity. Overall, the results highlight the potential of HAQ and its metal complexes as promising candidates for antioxidant and anticancer applications. These findings warrant further mechanistic studies and* in vivo *evaluations.*

Keywords: *ferron-azo ligand; lanthanide; transition metal complexes; antioxidant activity; cytotoxicity*

■ INTRODUCTION

Azo compounds, particularly those containing heterocyclic frameworks such as 8-hydroxyquinoline derivatives, have garnered more attention recently due to their diverse biological activities and wide-ranging applications in medicinal, analytical, and material sciences [1]. Among these, 8-hydroxyquinoline and its halogenated sulfonic acid derivatives are recognized for their potent antibacterial [2], antifungal [3], antioxidant [4], antiviral [5], and antiparasitic properties [6]. Furthermore, these compounds have demonstrated potential therapeutic benefits in neurodegenerative disorders, including Alzheimer's, Parkinson's, and Huntington's diseases [7].

One such derivative, ferron (8-hydroxy-7-iodoquinoline-5-sulfonic acid), has demonstrated significant biological efficacy and is often employed for its anti-amoebic and antiseptic properties [8]. The introduction of azo groups to such scaffolds not only enhances their physicochemical properties but also provides versatile coordination sites for metal ions, which facilitate the creation of stable, biologically active metal complexes [9]. Azo-metal complexes have gained prominence due to their roles in drug development, diagnostic imaging, and cancer therapy—especially in photodynamic applications where light-activated cytotoxicity enables targeted action [10]. Lanthanide and transition metal ions, such as La(III), Ce(IV), and Ni(II), possess unique coordination chemistry and redox behavior that can significantly influence the structural and biological profiles of ligand-based complexes [11]. Cerium(IV), for instance, exhibits reversible redox cycling (Ce^{4+}/Ce^{3+}) [12], which is advantageous in generating reactive oxygen species

(ROS)—a mechanism often exploited in anticancer and antioxidant strategies. Likewise, La(III) and Ni(II) centers contribute distinct thermal and electronic properties, enhancing the functionality and stability of the resulting complexes [13].

In light of these considerations, the current study reports the creation of an innovative azo ligand, namely 8-hydroxy-7-iodo-6-((4-sulfophenyl) diazinyl) quinoline-5-sulfonic acid (HAQ), via a diazotization–coupling reaction. The coordination behavior of HAQ with La(III), Ce(IV), and Ni(II) ions was systematically investigated. The resulting complexes were characterized by a comprehensive set of analytical and spectroscopic techniques, including elemental analysis, FTIR, UV-vis, ^{1}H-NMR, inductively coupled plasma (ICP), thermal gravimetric analysis (TGA), scanning electron microscopy (SEM), and X-ray diffraction (XRD). Moreover, their biological potential was evaluated in terms of antioxidant capacity using the phosphomolybdate assay and cytotoxicity against A549 lung carcinoma cells, providing insights into their structure–activity relationships and therapeutic relevance.

■ EXPERIMENTAL SECTION

Materials

All the chemicals and solvents employed were of reagent quality; no additional purification was necessary. The components included sodium hydroxide (Merck), sodium nitrite (Merck), nickel(II) acetate (Chemsavers), lanthanum chloride hydrate (Sigma-Aldrich), ceric sulfate (Sigma-Aldrich), ferron (BIOSYNTH), and *p*-aminosulfonic acid (Sigma-Aldrich).

Instrumentation

The Euro EA 3000 analyzer was used to do elemental analysis (C, H, and N). The Shimadzu FTIR-8400S spectrophotometer was used to record infrared spectra with CsI pellets within the range (200–4,000 cm^{-1}). UV-vis absorption spectra were acquired using a Shimadzu UV-1800 spectrophotometer in the range of 200–1,100 nm and a 10^{-4} M solution concentration. The SDT Q600 V20.9 instrument was used for TGA. Melting points were determined using a Stuart apparatus. NexION 5000 ICP-MS was used to determine the mass spectra (MS) of the compounds. The chloride content was measured using Mohr's technique. Magnetic susceptibility was measured at room temperature with an MSB-Auto balance. The ^{1}H-NMR spectra were acquired using a Bruker Avance III 400 MHz spectrometer with DMSO-d_6 as the solvent and TMS as the internal standard.

Procedure

Synthesis of HAQ ligand

The HAQ ligand was synthesized using diazotization-coupling techniques, as described in the literature [14]. A solution of *p*-amino sulfonic acid (0.01 mol, 0.173 g) in 10 mL of deionized water and 5 mL of glacial acetic acid was cooled to 0–5 °C. To create the diazonium salt, add a 10% sodium nitrite solution (10 mL) dropwise while stirring constantly. Separately, 0.01 mol (0.35113 g) of ferron was diluted in 10 mL of a 10% NaOH solution. The diazonium salt was gradually mixed into the alkaline solution while stirring. The pH was changed to 5–6 with acetic acid or NaOH, causing the orange product to precipitate. The substance was filtered, rinsed with a 1:1 water-ethanol mixture, and then dried (Scheme 1).

Synthesis of HAQ complexes

The lanthanum complex was synthesized in a 1:1 molar ratio (La:HAQ) by reacting $LaCl_3$ (0.001 mol, 0.3713 g) with an equimolar amount of HAQ (0.001 mol, 0.53528 g). In contrast, the nickel and cerium complexes were prepared in a 1:2 molar ratio (M:HAQ), using either $Ce(SO_4)_2$ (0.001 mol, 0.332 g) or $Ni(CH_3COO)_2$ (0.001 mol, 0.176 g) with HAQ (0.002 mol, 1.0704 g). Then, the resulting mixture is refluxed for 1 h with each metal ion alone, while monitoring the reaction progress

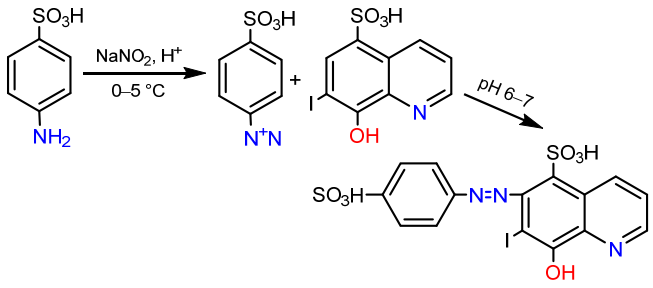

Scheme 1. Synthesis pathway of HAQ ligand

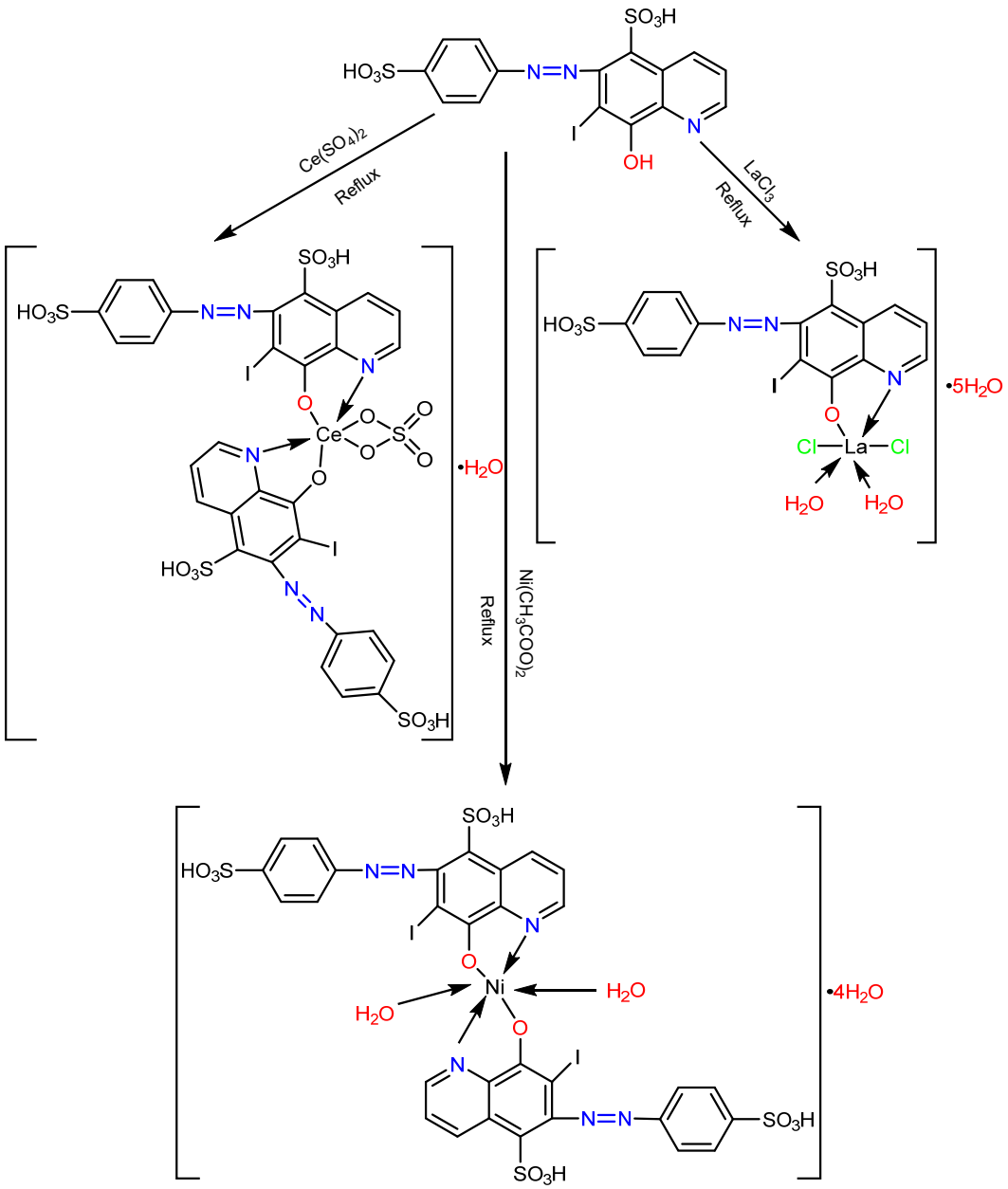

Scheme 2. Synthesis of the complexes

using TLC in the presence of solvent (methanol, ammonia, *n*-butanol = 0.8:1.2:4.0 mL). The colored precipitates were filtered, rinsed with a 1:1 ethanol-water solution, dried, and collected (Scheme 2).

Assessment of antioxidant activity

The HAQ ligand and its complexes were tested for antioxidant activity in the laboratory using a phosphomolybdate method [15]. Ascorbic acid was used as a standard to measure the total antioxidant capacity of fractions by the phosphomolybdate method. An aliquot of 0.1 mL of sample solution was mixed with 1 mL of reagent solution (0.6 M sulphuric acid, 28 mM sodium phosphate, and 4 mM ammonium molybdate). The tubes were capped and incubated in a water bath at 95 °C for 90 min. Following a 90-min temperature incubation, the samples were cooled to room temperature, and the absorbance of the mixture was measured at 765 nm on a spectrophotometer against a blank. A typical blank

consisted of 1 mL of the reagent solution and the correct volume of solvent and was incubated under the same conditions. As a standard, ascorbic acid was used [16].

Assessment of cytotoxic activity

The cytotoxicity of HAQ ligand and $[Ce(HAQ)_2(SO_4)]\cdot H_2O$ was investigated *in vitro* using the MTT test against lung cancer (A549) and normal dermal fibroblast (HdFn) cell lines [17]. Cells were cultured and maintained in 96-well plates using RPMI-1640 media at 37 °C and 5% CO_2. After reaching 70–80% confluence, cells were counted using a hemocytometer and then seeded in new plates. Cells were treated to repeated dilutions (25–400 µg/mL) of HAQ and cerium complex. After 24 h, the MTT solution was added and incubated for an additional 4 h. The formazan crystals were solubilized, and the absorbance was measured at 575 nm using an ELISA reader. The IC_{50} values were derived using cell viability percentages.

MnSOD and phosphorylated histone H2AX induction assay

HAQ was tested at two concentrations (100 and 200 µg/mL) in leukemia cell lines to assess the generation of ROS. To generate oxidative stress, 1 mM paraquat and 400 µg/mL iron citrate were utilized. Fixation, permeabilization, and antibody staining procedures were performed, followed by analysis using the ArrayScan HCS Reader [18].

■ RESULTS AND DISCUSSION

Physicochemical and Elements Analysis

The ligand HAQ was synthesized via a standard diazotization-coupling method using *p*-aminobenzenesulfonic acid and ferron. The resultant HAQ ligand and metal complexes with La(III), Ce(IV), and Ni(II) were produced in high yields. Table 1 summarizes the physical properties and elemental compositions of the synthesized compounds. The experimental values for carbon, hydrogen, and nitrogen were found to be consistent with the estimated values, validating the hypothesized stoichiometry. The detection of the synthesized complexes was accomplished through a molar conductivity study, which confirmed that they were the least non-electrolytic of them (Table 1).

FTIR Spectral Analysis

The FTIR spectrum of the azo ligand appears complex due to the presence of multiple functional groups, many of which exhibit overlapping vibrational regions. The major absorption bands of the free HAQ with its metal ion complexes are summarized in Table 2. The free HAQ ligand displays characteristic stretching vibrations assigned to the azo group ν(N=N), the C–N=N–C bond, and the sulfonic acid group ν(SO_3H) [19].

These bands largely remain unchanged in the spectra of the metal complexes, indicating that these groups are not directly involved in coordination. In some cases, however, slight shifts in intensity or position were observed upon complexation, which may reflect minor interactions or changes in molecular symmetry [20]. The stretching vibration of the hydroxyl (O–H) moiety in the quinoline appeared at 3438 and 3427 cm^{-1} in the free ligand spectrum. However, in the spectra of

Table 1. Physical and analytical properties of the ligand and its complexes

Compounds (M.wt (g/mol))	M:L	Color	(Experimental%) Theoretical%					Molar conductivity Λm (S mol^{-1} cm^2)
			C	H	N	M	Cl	
HAQ ($C_{15}H_{10}IN_3O_7S_2$) (535.28)	-	Dark brown	(33.15) 33.66	(2.47) 1.88	(8.48) 7.85	-	-	-
$[La(HAQ)Cl_2(H_2O)_2]\cdot 5H_2O$ (885.22)	1:1	Cherry	(20.84) 21.71	(2.71) 2.96	(5.71) 4.75	(16.11) 15.69	(7.89) 8.01	13
$[Ni(HAQ)_2(H_2O)_2]\cdot 4H_2O$ (1235.33)	1:2	Shiny brown	(28.48) 29.17	(3.05) 2.45	(7.07) 6.80	(5.39) 4.75	-	32
$[Ce(HAQ)_2(SO_4)]\cdot H_2O$ (1367.86)	1:2	Dark red	(21.60) 22.33	(2.14) 2.14	(5.67) 6.14	(10.58) 10.02	-	18

Table 2. The FTIR spectrum bands of the ligand and its complexes

Compounds	ν(OH)	ν(C=N)py	ν(SO_3H)	ν(N=N)azo	ν(-CN=NC-)	ν(H_2O)	ν(M-Cl)	(M-N)	(M-O)	(M-SO_4)
HAQ	3438	1623	1051	1504	1313	-	-	-	-	-
	3427	1593	sh, s	sh, s	m, sh					
	St. br.	1577								
		T,S								
[La(HAQ)$Cl_2(H_2O)_2$]·5H_2O	3454	1591	1049	1502 sh	1311	910	273	462	543	-
	3390	1562	Sh		M			S		
		d, w								
[Ni$(HAQ)_2(H_2O)_2$]·4H_2O	3446	1591	1049	1504	1301	918	-	439	518	-
	3419	1562								
		d,w								
[Ce$(HAQ)_2(SO_4)$]·H_2O	3508	1618	1049	1504	1315	918	-	441	543	599
	3496	w								

st =strong, br.= broad, s = small, m= medium, w= weak, vw = very weak, py = pyridine, d= double

Table 3. Thermal analysis data of the ligand and its complexes

Molecular formula (M.wt, g/mol)	Step	TG range of the decomposition (°C)	Suggested assignment	%Mass loss	
				%Calculated	%Found
HAQ ($C_{15}H_{10}IN_3O_7S_2$)	1	25–200	C_2H_4	5.23	5.27
(535.28)	2	200–450	C_4H_3	9.52	9.53
	3	450–750	C_5H_3	11.70	12.14
	4	750–900	$C_4N_3S_2O$	31.75	31.81
	5	Residue	IO_6	41.66	41.25
[La(HAQ)$Cl_2(H_2O)_2$]·5H_2O	1	25–250	$C_1H_{16}O_7$	15.81	15.80
(885.22)	2	250–400	C_7H_{10}	10.61	10.63
	3	400–750	$C_8Cl_2N_{1.5}O_{0.5}$	22.14	22.15
	4	750–900	$N_{1.5}S_2O_3$	15.02	15.07
	5	Residue	$LaIO_{3.5}$	36.35	36.34
[Ni$(HAQ)_2(H_2O)_2$]·4H_2O	1	25–150	$C_2H_{14}O_4$	8.26	8.27
(1235.33)	2	150–450	$C_{23}H_{16}O_2$	26.22	26.23
	3	450–750	$C_5N_5S_2O_4O_{0.25}$	21.20	21.28
	4	750–900	O_4S_2N	11.49	11.54
	5	Residue	$NiI_2O_5O_{0.75}$	32.70	32.69
[Ce$(HAQ)_2(SO_4)$]·H_2O	1	25–200	$C_4H_{17}O$	5.92	5.94
(1367.86)	2	200–400	$C_{20}H_{12}N$	19.44	19.48
	3	400–900	$C_9O_{14.5}S_5I_2N_5$	60.24	60.10
	4	Residue	$CeO_{3.5}$	14.38	14.48

the metal complexes, this band disappeared, suggesting coordination through the oxygen atom of the deprotonated hydroxyl moiety to the metal center [21]. Additionally, a stretching vibration band corresponding to the imine (C=N) moiety in the pyridine is observed at (1623,1593,1577) cm^{-1} in the ligand spectrum. This band exhibits changes in shape and position upon coordination with the study of metal ions. It represents evidence of coordination between the ligand and the metal ions, further supporting metal–ligand interaction through the nitrogen donor site [22], as illustrated in Fig. S1. Moreover, new bands appeared in the spectra of the complexes, which are attributed to metal ion bands with ligand vibrations, such as ν(M–O), ν(M–N py), and ν(M–Cl), confirming the formation of coordination bonds.

Thermogravimetric Analysis

To evaluate the thermal stability, TGA was performed, and the breakdown patterns and metal contents of the synthesized HAQ ligand and metal complexes are shown in Table 3 and Fig. S2. The thermal behavior was investigated in an inert argon environment at temperatures ranging from 25 to 1,000 °C with a constant heating rate of 10 °C/min. The TGA thermograms revealed multistep decomposition profiles, indicating that stepwise decomposition occurred, corresponding to the elimination of distinct ligand moieties before stable metal oxide residues were formed at the end of the heat degradation process [23].

The free ligand ($C_{15}H_{10}IN_3O_7S_2$) exhibited five unique weight loss stages. The early weight loss (25–200 °C) results in the release of adsorbed moisture and small molecular fragments, such as ethylene (C_2H_4) (weight loss 5.27%), indicating the removal of weakly bound moieties. The subsequent decomposition processes entailed fragmentation of the aromatic framework of the ligand, with considerable losses between 200–750 °C owing to the progressive breakdown of aromatic heterocyclic backbone (e.g., sulfonic acid, azo, and quinoline systems) with cumulative weight loss (52.48%). The last residue above (750 °C) supports the predicted chemical structure by indicating the presence of iodine and oxygen species, suggesting the formation of stable (IO_6), which accounts for 41.25% of the mass. These observations are consistent with the proposed molecular structure of HAQ [24].

The lanthanum complex $[La(HAQ)Cl_2(H_2O)_2]\cdot 5H_2O$ had four major breakdown stages. The first two phases (25–400 °C) removed coordinated and lattice water molecules, as well as organic ligand fragments ($C_{11}H_8$ and $C_5H_{18}O$). The ensuing steps (400–900 °C) resulted in the loss of coordinated chloride ions and ligand degradation, leaving a LaIO residue. The estimated and measured mass losses were in good agreement, supporting the suggested stoichiometry and coordination environment. Similarly, the nickel complex $[Ni(HAQ)_2(H_2O)_2]\cdot 4H_2O$ has five distinct decomposition steps. The initial weight loss was attributed to the elimination of hydration water (15.8% weight loss), followed by the gradual breakdown of the two coordinated HAQ ligands, including the cleavage of azo and sulfonic moieties. The ultimate residue, NiI_2O_5, indicates complete oxidation of the organic matrix and the retention of nickel and iodine in oxide form [25]. The cerium compound $[Ce(HAQ)_2(SO_4)]\cdot H_2O$ had a multi-stage breakdown profile. The first phase involves removing hydration water, then degrading organic components ($C_{20}H_{16}O$, $C_9O_{14}S_5I_2N_6H_8$), and releasing the sulphate group. The remaining product, CeO_4, indicates the synthesis of cerium(IV) oxide under oxidative circumstances. Overall, the TGA results corroborated the hypothesized molecular formulas and confirmed the effective coordination of HAQ with the relevant metal centers. The discovered heat stability and decomposition pathways shed light on the structural robustness and coordination geometry of the synthesized complexes [26]. Overall, the TGA results confirm the enhanced thermal stability of thermal complexes compared to the free ligand. The increased residue percentage and higher decomposition temperatures reflect the formation of thermally robust coordination frameworks involving metal-ligand interaction [27].

^{1}H-NMR Analysis

The ^{1}H-NMR spectra of the HAQ ligand were obtained in DMSO-d_6 (δ = 2.5 ppm) with TMS as an internal reference standard at 400–4000 MHz. The spectral data provided distinct chemical shifts (δ), expressed in parts per million (ppm), corresponding to the protons present in the molecular structure, thereby confirming the successful synthesis and structural integrity of the ligand, as depicted in Fig. S3 [28]. A singlet signal at 8.4 ppm indicates the proton of the sulfonic acid group ($-SO_3H$). The downfield shift is caused by the sulfonic acid group's strong electron-withdrawing nature, which exposes the proton and causes a greater chemical shift [29]. A singlet at 9.3 ppm represents the hydroxyl proton of the 8-hydroxyquinoline moiety. This signal occurs downfield as a result of intramolecular hydrogen bonding and the hydroxyl group's conjugation with the aromatic

quinoline ring [30]. Multiple counter signals at 7.0–8.5 ppm showed that the aromatic protons from conjugated benzene and quinoline rings contribute to these various peaks. The multiplicity and chemical shift values are consistent with the expected chemical environment for protons in a strongly conjugated aromatic system with electron-withdrawing substituents, such as iodine and azo (–N=N–) groups [31].

UV-vis Spectroscopy and Magnetic Properties

The UV-vis spectrum of HAQ, as shown in Fig. S4 and summarized in Table 4, revealed two distinct absorption bands: A broad shoulder at 410 nm ascribed to n→π* transitions involving the nonbonding electrons of nitrogen and oxygen atoms from (OH, N=N, and SO_3H) moieties. These transition characteristics of azo compounds bearing electron-rich hetero atoms [32]. A sharp band at 291 nm for π→π* transitions within the aromatic and conjugated system, primarily from the quinoline and azo moieties [33]. Bathochromic shifts and new charge transfer (CT) bands were observed in the spectra of the La(III) and Ce(IV) complexes after complexation, confirming successful coordination within dia management properties and an octahedral geometry [34]. The paramagnetic Ni(II) complex also displayed mild *d-d* transitions at 431 nm, which are indicative of octahedral geometry [35]. According to the Tambe-Sugano diagram for d^8 ions, this band is tentatively assigned to the $^3A_2g \rightarrow {}^3T_2g$ (p) transition [36]. The bathochromic shifts in the absorption maxima of the metal complexes relative to the free ligand support the successful coordination of HAQ with metal centers. These spectral modifications are consistent with increased delocalization and altered ligand field environments upon complex formation [37].

Scanning Electron Microscopy

SEM analysis was employed to characterize the morphological properties of the surface and the microstructural features of the free ligand and its Ce-complex. The research sheds light on particle shape, surface roughness, and crystallinity, all of which have a significant impact on physicochemical and biological behavior [38]. The SEM image of the free HAQ ligand, as illustrated in Fig. S5, revealed an uneven, heterogeneous surface made up of loosely packed particles with amorphous properties. This chaotic shape indicates low crystallinity and a lack of long-range structural organization, which is consistent with its molecular origin prior to coordination with cerium ions. Surface characteristics changed noticeably after complexation [39]. Ce(IV) complex, $[Ce(HAQ)_2(SO_4)]\cdot H_2O$ had a unique morphology, with a porous, sponge-like texture and uneven surface. This variance may be due to steric hindrance and the high oxidation state of Ce(IV), as well as the existence of sulphate anions, which could impair uniform crystal formation. These morphological distinctions between the free ligand and Ce-complex demonstrate effective coordination and lend support to the creation of architecturally different supramolecular structures. The Ce-complex's improved surface regularity and compactness are anticipated to affect its thermal stability and biological activity (Table 5) [40].

X-ray Diffraction

The free HAQ ligand and its cerium(IV) complex $[Ce(HAQ)_2(SO_4)]\cdot H_2O$ were analyzed using XRD to determine their crystalline structure and average

Table 4. Electronic transition and magnetic properties data of the ligand and its complexes

Compounds	λ (nm)	Wavenumber (cm^{-1})	Assignment	μ (B.M)
HAQ	410	24.390	n→π*	-
	291	34.364	π→π*	
$[La(HAQ)Cl_2(H_2O)_2]\cdot 5H_2O$	487	20.533	CT	0
$[Ni(HAQ)_2(H_2O)_2]\cdot 4H_2O$	431	23.202	CT	2.8
			$^3A_2g \rightarrow {}^3T_1g$ (p)	
$[Ce(HAQ)_2(SO_4)]\cdot H_2O$	492	20.325	CT	0

Table 5. SEM data of the ligand and Ce-HAQ complex

Compounds	Average radii (nm)	Shape
HAQ	22.440	Heterogenous coral
$[Ce(HAQ)_2(SO_4)]\cdot H_2O$	42.707	Heterogenous spherical

crystallite size. This approach gives critical information regarding structural ordering at the nanoscale, which directly affects the compounds' physicochemical properties. The XRD pattern of the free HAQ ligand showed a broad diffraction peak centered at 2θ = 31.83° and a full width at half maximum (FWHM, β) of 0.1968 radians. The broadness of the peak indicates low crystallinity or partially amorphous character, which is common in organic compounds with uneven molecular packing. The crystallite size was estimated by applying the Debye-Scherrer equation [41] in Eq. (1);

$$D = \frac{K\lambda}{\beta \cos\theta} \quad (1)$$

where D is the average crystallite size, K is the shape factor (typically 0.9), λ is the wavelength of Cu Kα radiation (1.5406 Å), β is the FWHM (in radians), and θ is the Bragg angle. The predicted crystallite size for the HAQ ligand was 7.14 nm, indicating that the material is nanocrystalline or semi-amorphous. The Ce(IV) complex had a sharper and narrower peak at 2θ = 31.87° with β = 0.1476 radians, indicating a predicted crystallite size of 9.51 nm, as was shown in Fig. S6 and Table 6. The lowered peak width and increased crystallite size indicate a greater degree of crystallinity after interaction with the metal ion. The addition of cerium and the development of the chelated complex are anticipated to promote more regular molecular packing and long-range organization within the solid phase [42].

These findings demonstrate that complexation with Ce(IV) significantly alters the structural organization of the HAQ ligand, leading to improved crystallinity and a more ordered lattice structure. The increase in crystallite size may also contribute to enhanced thermal stability and biological activity, as supported by complementary characterization techniques [43]. Interplanar spacing (*d*) was calculated based on the use of the most intense peak following Bragg's law in Eq. (2) [44];

$$n\lambda = 2d\sin\theta \quad (2)$$

where λ = 0.15406 Å, n is the integer number, *d* is the spacing between crystal layers (the path difference), and θ is the incident angle (the angle between the incoming ray and the scattering plane).

Mass Spectroscopy

The GC-MS analysis of the HAQ ligand fragmentation behavior is shown in Fig. S7. The spectrum revealed a prominent molecular ion peak at *m/z* = 535.2, which corresponds to the intact molecular weight of HAQ ($C_{15}H_{10}IN_3O_7S_2$), thereby validating that the proposed HAQ ligand was present. This analysis was performed to confirm its molecular structure and assess its molecular formula. In addition to the molecular ion peak, several significant fragment peaks were observed, arising from the stepwise cleavage of characteristic functional groups.

The base peak appeared at *m/z* = 105.0, indicating a highly stable fragment, likely derived from the *p*-sulfophenyl moiety after cleavage of the azo (–N=N–) bond. This fragment is commonly reported in the fragmentation of sulfonated aromatic azo compounds, as it offers strong resonance stabilization. Fragmentation pathways suggest that the ligand undergoes homolytic and heterolytic bond cleavages at labile sites, notably: The N=N azo bridge, which is prone to cleavage due to its conjugated yet relatively weak double bond. The C–S and S=O bonds within the sulfonic acid group, which may break under electron impact, generating distinct sulfur- and oxygen-containing fragments. Halogen loss (iodine atom, I) may also occur, producing a characteristic peak due to the heavy atomic mass of iodine (I = 127 amu). The fragmentation pattern, summarized in the proposed scheme (Scheme 3), supports the presence of key functional groups, including quinoline, phenolic OH, sulfonic acid, iodine, and azo linkages. The fragmentation behavior is consistent with literature reports on structurally similar hydroxyquinoline-based azo compounds [45].

Table 6. XRD for HAQ ligand and $[Ce(HAQ)_2(SO_4)]\cdot H_2O$

Compounds	2θ	FWHM (nm)	D (nm)	d (Å)	
				Calculated	Found
HAQ	31.83	0.19	7.14	2.73	2.81
$[Ce(HAQ)_2(SO_4)]\cdot H_2O$	31.87	0.14	9.51	2.73	2.80

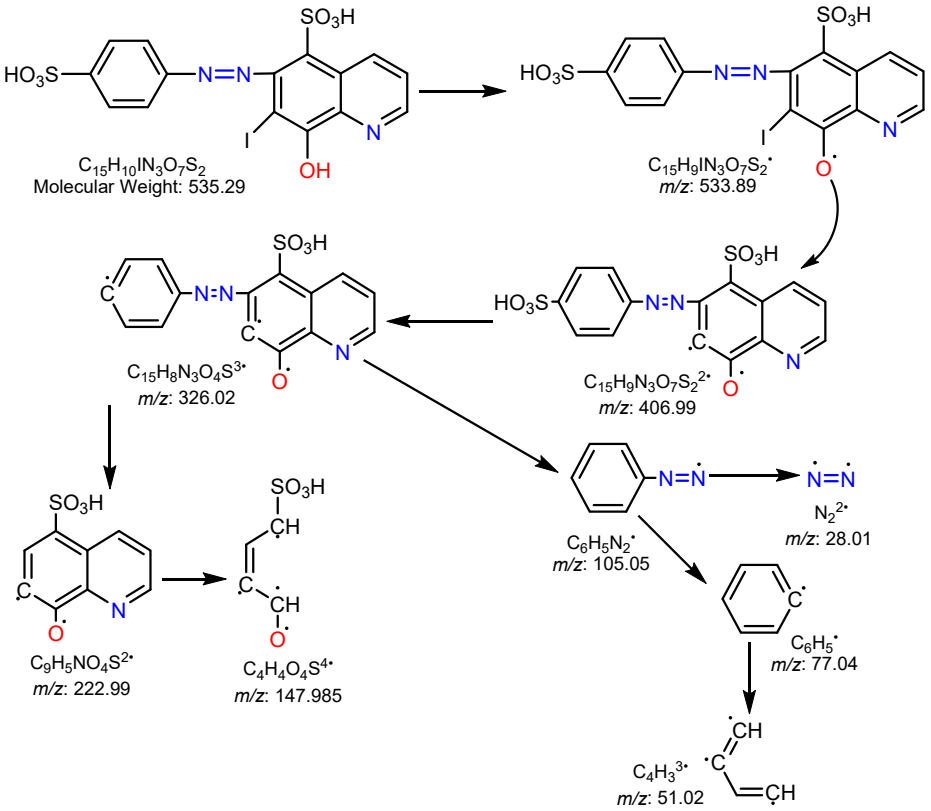

Scheme 3. Fragmentation of the HAQ ligand

Antioxidant Activity

The antioxidant capability of the free HAQ ligand and its metal complexes was evaluated using the phosphomolybdate test, a well-established spectrophotometric technique for determining total antioxidant capacity (TAC). This approach involves reducing Mo(VI) to Mo(V) in the presence of antioxidants, resulting in a green phosphate/Mo(V) combination with maximum absorption at 765 nm [16]. All examined compounds had detectable antioxidant activity, with variations due to differences in molecular structure, electron-donating capacity, and metal coordination. The HAQ ligand demonstrated a strong ability to decrease Mo(VI), most likely due to the presence of phenolic-OH and azo groups, which are known to participate in redox processes by donating electrons or hydrogen atoms to ROS. Changes in antioxidant activity were detected following complexation with metal ions. Specifically, the Ce(IV) complex $[Ce(HAQ)_2(SO_4)]\cdot H_2O$ showed higher antioxidant potential compared to the free ligand. This enhancement may be ascribed to the redox-active nature of Ce(IV), which can undergo facile Ce(IV)/Ce(III) interconversion, thus amplifying its capacity to scavenge free radicals or facilitate electron transfer reactions. Furthermore, coordination with the metal center may stabilize the ligand structure and enhance its ability to interact with oxidizing species. The antioxidant effectiveness is tabulated in Table 7. This suggests that the incorporation of metal ions not only enhances the structural rigidity of the ligand but also

Table 7. The antioxidant potential was determined by utilizing the following formula

Items	Concentration (μg/mL)		
	150	100	50
Blank		0.004±0.002	
Control	0.13 ± 0.002	0.12 ± 0.002	0.14 ± 0.002
HAQ	27.27 ± 1.005	21.58 ± 0.310	15.75 ± 0.610
$[La(HAQ)Cl_2(H_2O)_2]\cdot 5H_2O$	26.17 ± 0.500	19.58 ± 0.460	10.75 ± 7.170
$[Ni(HAQ)_2(H_2O)_2]\cdot 4H_2O$	26.28 ± 0.360	22.80 ± 0.680	15.52 ± 0.720
$[Ce(HAQ)_2(SO_4)]\cdot H_2O$	26.70 ± 0.690	22.04 ± 0.400	16.43 ± 0.500

introduces additional redox centers that can improve overall antioxidant behavior [46].

Evaluation of Cytotoxic Activity

The cytotoxic potential of the synthesized HAQ ligand and its cerium complex $[Ce(HAQ)_2(SO_4)]\cdot H_2O$ was tested *in vitro* using the MTT assay against human lung carcinoma cell line (A549) and normal human dermal fibroblast cells (HdFn) [47]. The MTT assay is a colorimetric approach that uses mitochondrial dehydrogenases to reduce tetrazolium salt MTT to formazan in live cells. The absorbance at 575 nm indicates cell viability. Both the free ligand and its Ce(IV) complex demonstrated dose-dependent cytotoxicity against A549 cells, with a stronger impact found at higher doses. The HAQ ligand showed considerable antiproliferative activity (IC_{50} = 52.75 μg/mL), while the Ce(IV) complex had slightly lesser cytotoxic potency (IC_{50} = 176.2 μg/mL) as directed in Tables 8–9 and Fig. S8. These data imply that the HAQ ligand may interfere with cellular redox homeostasis or DNA replication, most likely through its azo and phenolic functional groups, which are known to cause oxidative stress and impair cellular function. Interestingly, both compounds demonstrated significantly lesser toxicity towards normal HdFn cells, with IC_{50} values of 152.4 μg/mL for HAQ and 193.9 μg/mL for Ce(IV) complex. This selectivity suggests that the chemicals may preferentially target quickly dividing cancer cells while sparing normal healthy cells, which is an attractive feature for anticancer prospects. The substantially decreased cytotoxicity of the Ce(IV) complex compared to the free ligand could be due to a decrease in free functional groups during coordination or a modification of ligand reactivity during complexation. However, the complex still maintains a high level of activity, probably due to the cerium center's redox characteristics, which may contribute to ROS production and apoptotic signaling in cancer cells [18].

Table 9. Cytotoxicity effect of HAQ ligand

Conc. (μg/mL)	HAQ
DMSO	384.0 ± 27.22
50	448.0 ± 18.68
100	581.3 ± 11.06
200	742.7 ± 8.02

Table 8. Cytotoxic effect of HAQ ligand and $[Ce(HAQ)_2(SO_4)]\cdot H_2O$ on lung cancer cell line (A549) and normal cell line

Concentration (μg/mL)	Cell viability			
	HAQ		$[Ce(HAQ)_2(SO_4)]\cdot H_2O$	
	HdFn	A549	HdFn	A549
	Mean ± SD	Mean ± SD	Mean ± SD	Mean ± SD
400	69.83 ± 2.31	36.14 ± 1.28	76.81 ± 1.18	51.77 ± 1.91
200	76.73 ± 1.28	42.63 ± 2.03	88.19 ± 1.10	67.16 ± 1.73
100	88.69 ± 1.57	53.74 ± 1.87	91.74 ± 1.26	87.42 ± 3.38
50	93.71 ± 0.17	62.96 ± 2.43	94.09 ± 0.30	93.82 ± 0.54
25	95.17 ± 0.35	77.31 ± 1.51	95.91 ± 0.29	95.56 ± 0.24

■ CONCLUSION

This study developed an efficient method for synthesizing and characterizing a new azo-based ligand (HAQ) derived from 8-hydroxyquinoline using various analytical and spectroscopic techniques. The ligand was complexed with La(III), Ni(II), and Ce(IV) ions to form stable metal complexes, confirmed by thermal and structural analyses. The complexes showed higher thermal stability and distinct morphological features compared to the free ligand. Biological studies revealed notable antioxidant activity, with the Ce(IV) complex showing the strongest effect, and selective cytotoxicity against A549 lung cancer cells. Overall, HAQ and its metal complexes demonstrate promising antioxidant and anticancer potential for future pharmaceutical applications.

■ ACKNOWLEDGMENTS

The authors thank the University of Baghdad for its support of this research project.

■ CONFLICT OF INTEREST

There are no conflicts of interest to declare.

■ AUTHOR CONTRIBUTIONS

Noora Qasem Muhi and Alyaa Khider Abbas contributed to the research design, conducted the experimental work, interpreted the results, drafted the manuscript, reviewed, and approved the final version of the manuscript.

■ REFERENCES

[1] Alghuwainem, Y.A.A., Abd El-Lateef, H.M., Khalaf, M.M., Abdelhamid, A.A., Alfarsi, A., Gouda, M., Abdelbaset, M., and Abdou, A., 2023, Synthesis, structural, DFT, antibacterial, antifungal, anti-inflammatory, and molecular docking analysis of new VO(II), Fe(III), Mn(II), Zn(II), and Ag(I) complexes based on 4-((2-hydroxy-1-naphthyl)azo) benzenesulfonamide, *J. Mol. Liq.*, 369, 120936.

[2] Abd El-Lateef, H.M., Khalaf, M.M., Gouda, M., Amer, A.A., Abdelhamid, A.A., and Abdou, A., 2024, Design, synthesis of new mixed azo-hydroxyquinoline complexes; *in vitro* anti-inflammatory, antifungal, antibacterial, theoretical, and molecular docking interactions investigation, *J. Mol. Struct.*, 1307, 138016.

[3] Rahman, M.M., Haque, T.M.A., Sourav, N.S., Rahman, S., Yesmin, S., Mia, R., Al Noman, A., and Begum, K., 2021, Synthesis and investigation of dyeing properties of 8-hydroxyquinoline-based azo dyes, *J. Iran. Chem. Soc.*, 18 (4), 817–826.

[4] Abdel-Kader, N.S., Abdel-Latif, S.A., El-Ansary, A.L., and Hemeda, M.A., 2024, Design, synthesis, spectroscopic studies, DFT, TD-DFT/PCM calculations, and molecular docking studies on the anti-SARS and anti-COVID-19 activities of novel benzidine bis azo 1-(2-hydroxy-3-naphthoic acid) complexes with some transition metal ions, *Polycyclic Aromat. Compd.*, 44 (6), 3601–3632.

[5] Martín-Montes, Á., Jimenez-Falcao, S., Gómez-Ruiz, S., Marín, C., and Mendez-Arriaga, J.M., 2023, First-row transition 7-oxo-5-phenyl-1,2,4-triazolo[1,5-a]pyrimidine metal complexes: antiparasitic activity and release studies, *Pharmaceuticals*, 16 (10), 1380.

[6] Joaquim, A.R., Pippi, B., de Cesare, M.A., Rocha, D.A., Boff, R.T., Staudt, K.J., Ruaro, T.C., Zimmer, A.R., de Araújo, B.V., Silveira, G.P., Martins, A.F., Teixeira, M.L., dos Santos, F.P., Fuentefria, A.M., and de Andrade, S.F., 2019, Rapid tools to gain insights into the interaction dynamics of new 8-hydroxyquinolines with few fungal lines, *Chem. Biol. Drug Des.*, 93 (6), 1186–1196.

[7] Majidian, M., Raoof, J.B., Hosseini, S.R., Fischer, J., and Barek, J., 2020, Determination of 8-hydroxy-7-iodo-5-quinoline sulfonic acid (HIQSA) at renewable electrode with Sb_2O_3/MWCNT-TiO_2 nanohybrid, *J. Electroanal. Chem.*, 858, 113775.

[8] Soliman, A.Q.S., Abdel-Latif, S.A., Abdel-Khalik, S., Abbas, S.M., and Ahmed, O.M., 2024, Design, synthesis, structural characterization, molecular docking, antibacterial, anticancer activities, and density functional theory calculations of novel Mn^{II}, Co^{II}, Ni^{II}, and Cu^{II} complexes based on pyrazolone-sulfadiazine azo-dye ligand, *J. Mol. Struct.*, 1318, 139402.

[9] Eltaboni, F., Bader, N., El-Kailany, R., Elsharif, N., and Ahmida, A., 2022, Chemistry and applications

of azo dyes: A comprehensive review, *J. Chem. Rev.*, 4 (4), 313–330.

[10] Juvekar, V., Lim, C.S., Lee, D.J., Park, S.J., Song, G.O., Kang, H., and Kim, H.M., 2021, An azo dye for photodynamic therapy that is activated selectively by two-photon excitation, *Chem. Sci.*, 12 (1), 427–434.

[11] Ghani, A.H., and Alabdali, A.J., 2022, Synthesis, characterization and anti-cancer activity of gold(III) and nickel(II) metal ion complexes derived from tetrazole–triazole compound, *Al-Nahrain J. Sci.,* 25 (2), 8–13.

[12] Bao, G., Wen, S., Lin, G., Yuan, J., Lin, J., Wong, K.L., Bünzli, J.C.G., and Jin, D., 2021, Learning from lanthanide complexes: The development of dye-lanthanide nanoparticles and their biomedical applications, *Coord. Chem. Rev.*, 429, 213642.

[13] Abo El-Maali, N., Wahman, A.Y., Aly, A.A.M., Nassar, A.Y., and Sayed, D.M., 2020, Anticancer activity of lanthanum(III) and europium(III) 5-fluorouracil complexes on Caco-2 cell line, *Appl. Organomet. Chem.*, 34 (6), e5594.

[14] Benkhaya, S., M'rabet, S., and El Harfi, A., 2020, Classifications, properties, recent synthesis and applications of azo dyes, *Heliyon*, *6* (1), e03271.

[15] Umamaheswari, M., and Chatterjee, T.K., 2008, *In vitro* antioxidant activities of the fractions of *Coccinia grandis* L. leaf extract, *Afr. J. Tradit., Complementary Altern. Med.*, 5 (1), 61–73.

[16] Prieto, P., Pineda, M., and Aguilar, M., 1999, Spectrophotometric quantitation of antioxidant capacity through the formation of a phosphomolybdenum complex: Specific application to the determination of vitamin E, *Anal. Biochem.*, 269 (2), 337–341.

[17] Bhat, M., and Marar, T., 2015, Cytotoxic effect of purified L-asparaginase from *Salinicoccus* sp. M KJ997975, *Int. J. Curr. Microbiol. Appl. Sci.*, 4 (4), 701–712.

[18] Al-Jumaily, E.F., Al-Shanon, A.F., and Al-Barzanchi, S.I., 2015, Antioxidant and reactive oxygen species induction using purified natural lignan dimmer isolated from *Myristica fragrans* seed, *World J. Pharm Res.*, 4 (3), 314–324.

[19] Adeniyi, A.O., Boyro, D.E.A., Chindo, I.Y., and Mahmoud, A.A., 2023, Spectrophotometric and infra-red analyses of azo reactive dyes derived from 2-methyl-3-(2'-methylphenyl)-6-arylazo-4-oxoquinazoline, *Sci. World J.*, 18 (2), 231–239.

[20] Abdel-karim, A.M., Shahen, S., and Gaber, G., 2021, 4-Aminobenzenesulfonic acid as effective corrosion inhibitor for carbon steel in hydrochloric acid, *Egypt. J. Chem.*, 64 (2), 825–834.

[21] Din Kadhoum Alzamili, S., Shamran Mohammed, H., and Mothhar Muslim, T., 2025, Biological activity of azo quinoline dye and its palladium(II) complex, *Bull. Chem. Soc. Ethiop.*, 39 (1), 91–100.

[22] Abbas, R.A., Jarad, A.J., Nafliu, I.M., and Nechifor, A.C., 2019, Synthesis, characterization and antibacterial activity from mixed ligand complexes of 8-hydroxyquinoline and tributylphosphine for some metal ions, *Rev. Chim.*, 70 (1), 36–40.

[23] Li, F.H., Liu, S.H., Guo, R.L., and Hou, H.Y., 2023, Thermal stability and decomposition mechanism analysis of 1,1'-azobis (cyclohexanecarbonitrile) by STA, DSC, ARC and TG-FTIR, *J. Loss Prev. Process Ind.*, 83, 105044.

[24] Diab, M.A., El-Sonbati, A.Z., Gomaa, E.A., El-Mogazy, M.A., Morgan, S.M., Abou-Dobara, M.I., Omar, N.F., El-Zahed, M., and Osman, M.A., 2022, Polymer complexes: LXXIX—synthesis, characterization, geometrical structures, biological activity and molecular docking studies of azo dye complexes, *J. Iran. Chem. Soc.*, 19 (7), 3079–3102.

[25] Ahmed, A.A., Peter, J.O., and Ngaramu, F.A.B., 2021, Synthesis and characterization of mixed ligand metal(II) complexes with Schiff base and 8-hydroxyquinoline as ligands, *J. Chem. Lett.*, 2 (1), 43–49.

[26] Manulla, M.H., and Abbas, A.K., 2025, La(III) and Ce(IV) complexes of novel azo-theophylline ligand: Structural analysis and biological effectiveness, *Iraqi J. Sci.*, 66 (1), 39–51.

[27] Hassan, A., Hemida, E., Mahmoud, N.I., Kamel, M., Elsharkawy, H.M., Khalil, A.S.G., Abdel-Hafiez, M., and Saber, M.R., 2025, Synthesis, structural characterization, and magnetic properties of two

new Fe(III)Mn(III) 1D bimetallic compounds, *ACS Omega*, 10 (8), 8271–8280.

[28] Mohammed Noori Khaleel, A., 2025, Synthesis of indole borate ligand with Ni(II) and Cu(II) complexes, *Bull. Chem. Soc. Ethiop.*, 39 (4), 703–712.

[29] Manulla, M.H., and Abbas, A. K., 2025, Design and structural characterization of novel azo-theophylline as acid-base indicator, *Ibn AL-Haitham J. Pure Appl. Sci.*, 38 (2), 266–277.

[30] Alzamili, S.D.K., Mohammed, H.S., and Muslim, T.M., 2025, Biological activity of azo quinoline dye and its palladium(II) complex, *Bull. Chem. Soc. Ethiop.*, 39 (1), 91–100.

[31] Yildiz, E.A., Pepe, Y., Erdener, D., Karatay, A., Boyacioglu, B., Ünver, H., Yapar, G., Demir, N., Yıldız, M., and Elmali, A., 2023, Colorimetric chemical sensing properties of 3-amino-4-hydroxybenzenesulfonic acid-based Schiff bases containing electron donor–acceptor groups, *Chem. Phys.*, 574, 112048.

[32] Taher, D., AlNaimat, S., Assaf, K.I., Helal, W., and Korb, M., 2025, Synthesis of chloro-substituted β-ketiminate palladium complexes, spectral and thermal investigation of their structures, *Eur. J. Inorg. Chem.*, 28 (6), e202400730.

[33] Radhi, E.R., Ali, F.J., and Ali, K.J., 2023, Synthesis and characterization of a new azo quinoline ligand and its metal complexes with spectrophotometric determination and biological efficacy study of its Hg(II) complex, *Bull. Chem. Soc. Ethiop.*, 37 (6), 1423–1433.

[34] Al-mizher, T.T., and Abbas, A.K., 2025, Synthesis, identification, and biological evaluation of some metal ions complexes derived from thymine-azo ligand, *Indones. J. Chem.*, 25 (3), 853–863

[35] Al-Saidi, H.M., Gouda, G.A., Abdel-Hakim, M., Alsenani, N.I., Alfarsi, A., Mahross, M.H., Farghaly, O.A., and Hosny, S., 2022, Synthesis and characterization of Ni(II), Cu(II), Zn(II) and azo dye based on 1,10-*o*-phenanthroline binary complexes: corrosion inhibition properties and computational studies, *Int. J. Electrochem. Sci.*, 17 (3), 220333.

[36] Al-Zahraa, F., and Al-Hamdani, A.A.S., 2024, Synthesis, characterization, thermal studies, and antioxidant activities of azo dye[2-[(3-hydroxyphenyl)diazinyl]-1,2-benzothiazol-3(2*H*)-one-1,1-dioxide] and metal ion complexes, *Iraqi J. Sci.*, 65 (12), 6842–6861.

[37] Mustapha, B., Saleh, A.A., El-Seifat, R., Bufarwa, S., Hasan, H., and Moustafa, D., 2025, Exploring the antituberculosis, anti-inflammatory, and antimicrobial activities and computational potential of quinoline-8-ol azo dye complexes, *Appl. Organomet. Chem.*, 39 (8), e70310.

[38] Al-Adilee, K.J., and Hasan, S.R., 2021, Synthesis, characterization and biological activity of heterocyclic azo-Schiff base ligand derived from 2-amino-5-methyl thiazol and some transition metal ions, *IOP Conf. Ser.: Earth Environ. Sci.*, 790 (1), 012031.

[39] Jedidi, I., Khemakhem, S., Saïdi, S., Larbot, A., Elloumi-Ammar, N., Fourati, A., Charfi, A., Ben Salah, A., and Ben Amar, R., 2011, Preparation of a new ceramic microfiltration membrane from mineral coal fly ash: Application to the treatment of the textile dying effluents, *Powder Technol.*, 208 (2), 427–432.

[40] Mahmood, A.A., Hammadi, O.A., and Ibraheem, K.R., 2022, Preparation and photoluminescence spectra of organometallic complexes containing nanoparticles as random gain media, *Indones. J. Chem.*, 22 (1), 205–211.

[41] Jahan Tamanna, N., Sahadat Hossain, M., Mohammed Bahadur, N., and Ahmed, S., 2024, Green synthesis of Ag_2O & facile synthesis of ZnO and characterization using FTIR, bandgap energy & XRD (Scherrer equation, Williamson-Hall, size-train plot, Monshi-Scherrer model), *Results Chem.*, 7, 101313.

[42] Abbas, N.F., and Abbas, A.K., 2020, Novel complexes of thiobarbituric acid–azo dye: Structural, spectroscopic, biological activity and dying, *Biochem. Cell. Arch.*, 20 (1), 2419–2433.

[43] Fifere, N., Ardeleanu, R., Doroftei, F., Dobromir, M.,

and Airinei, A., 2024, Tailoring the structural and optical properties of cerium oxide nanoparticles prepared by an ecofriendly green route using plant extracts, *Int. J. Mol. Sci.*, 25 (1), 681.

[44] Stepanov, S., 2021, New developments including X-ray standing waves in the dynamical Bragg diffraction program of X-ray server, *J. Appl. Crystallogr.*, 54 (5), 1530–1534.

[45] Talal Ali Al-Rubaye, N., and Ali Salih Al-Hamdani, A., 2025, Synthesizing, characterization of some metal ion complexes with new azo dye and studying antioxidant and anticancer (MCF-7), *Bull. Chem. Soc. Ethiop.*, 39 (5), 859–875.

[46] Banavar, S., Deshpande, A., Sur, S., and Andreescu, S., 2021, Ceria nanoparticle theranostics: Harnessing antioxidant properties in biomedicine and beyond, *J. Phys.: Mater.*, 4 (4), 042003.

[47] Noriega, P., Gortaire, G., and Osorio, E., 2021, "Mass Spectrometry and Its Importance for the Analysis and Discovery of Active Molecules in Natural Products" in *Natural Drugs from Plants*, Eds. El-Shemy, H., IntechOpen, London, UK.